Factor Analysis in Prostate Cancer: Delineation of Organ Structures and Automatic Generation of In- and Output Functions

Christiaan Schiepers, Carl K. Hoh [*], Johan Nuyts [#], *Member IEEE*, Hsiao-Ming Wu, Michael E. Phelps, and Magnus Dahlbom, *Senior Member IEEE*

***Abstract*--: Factor Analysis (FA) is used for extracting the properties of dynamic sets. *Objective*: FA was applied to dynamic studies using Positron Emission Tomograpy (PET) to create factor images and factor curves from which input and output functions could be derived for kinetic modeling. This non-invasive, automated, and image based analysis should permit routine application of quantitative PET in cancer patients. *Methods:* In 9 men with prostate cancer, dynamic PET studies were performed on an ECAT HR+ system. After administration of 13.5 mCi of ^{11}C labeled acetate, data were acquired for 20 min. Images were reconstructed with iterative algorithms, a maximum a posteriori (MAP) for transmission scans, and ordered subset expectation maximization (OSEM) for emission scans. Body contour was determined with thresholding of the transmission images. All voxels included in the body contour were used for processing. FA extracted the shape of the pure time activity curves (TACs). The factors were used to create functional images, from which a region-of-interest (ROI) could be generated with thresholding techniques. These ROIs were used to create image-based TACs. *Results:* The automated procedure was successful in 8/9 patients. Minimal intervention generated reliable factors in the remaining patient. Factors are normalized; their magnitude was adjusted by a scale factor using: 1) reversed normalization, 2) image-based parameters. In principle, the input factor generated by FA has no spillover and produces a pure vascular image and curve. Factor images provided diagnostic information on tumors. The method is operator independent and reproducible. *Conclusion:* The automated procedure generated factors from dynamic PET data corresponding to vessels and tumor. FA can non-invasively generate input and output functions. This processing tool facilitates PET as a reproducible quantification method in routine oncological applications.**

I. Introduction

One of the unique features of Positron Emission Tomography (PET) is the accurate quantification of metabolic processes in-vivo. This requires the measurement of a so-called input function, i.e. clearance of injected tracer from the blood, and an output function, i.e. uptake of tracer in the organ or structure of interest. The input function can be derived from images if a large vascular structure is in the field of view. Otherwise, invasive methods have to be used, e.g. blood sampling from an artery, a labor-intensive procedure with a small risk of complications. A non-invasive, automated, image-based method of generating input and output functions would be patient friendly, efficient, and would allow quantitative PET to be applied routinely.

Factor analysis (FA) has been used to distinguish functional parameters in dynamic image sets. FA has been proposed some time ago [1], but the perceived mathematical difficulty [2] has limited its use [3]. Initially, computing time was long, but current computer speed permits FA to be performed in a few minutes. An implementation of our method has been reported earlier [4]. We have presented data in osteoporosis [5], and were able to derive input functions that provided accurate values of bone flow and fluoride influx rate. Also data on breast and prostate cancer with FDG as tracer were reported [6].

Here we describe the implementation of a fully automated procedure, without operator intervention during the processing steps. It produces an input function, describing the disappearance of tracer from the vascular pool, and an output function, describing tracer uptake in the prostate cancer. These functions serve as input for the kinetic modeling program, which calculates the diffusion constants between compartments with non-linear regression. During processing, factor images are created that are parametric representations of the temporal changes in the study. In this way, FA can be viewed as a data reduction method. A factor has diagnostic value by highlighting the dynamic behavior of the tracer in the structure of interest, and by presenting this information for all voxels of the dynamic set in a single functional image.

II. Methods

Population: Six men with primary prostate cancer and three with prostate cancer relapse were studied. They fasted for at least 4 hr. before the study. After positioning of the pelvis in the scanner with the prostate gland in the approximate center field of view, 13.5 mCi of ^{11}C labeled acetate was injected and PET imaging started simultaneously.

Acquisition: All studies were performed with an ECAT HR+ scanner (Siemens/CTI, Knoxville, TN). A dynamic emission scan was acquired over 20 min. and consisted of 28 frames of 12x10, 9x20, 5x60, 2x300 sec duration. A trans-

Submitted November 28, 2001

Christiaan Schiepers, is with UCLA School of Medicine, Los Angeles, CA 90095 USA (telephone 310-825-8892, e-mail: cschiepers@mednet.ucla.edu). Christine Wu, Michael Phelps and Magnus Dahlbom are also at UCLA School of Medicine.

Carl Hoh[*] is with UCSD School of Medicine, San Diego, California USA (telephone: 619-543-6681, e-mail: ckhoh@ucsd.edu).

Johan Nuyts[#] is with the Katholieke Universiteit, Leuven, Belgium (telephone: +32-16-3715, e-mail: johan.nuyts@med.kuleuven.ac.be).

Figure 1. Typical transmission plane with photopenic area related to air in the bowel (left). Thresholding removes the bed (middle). All voxels are used for further processing by filling-in the inside (right).

mission scan of 20 min was acquired to correct for attenuation effects. The images were reconstructed with iterative algorithms (method UCLA-KUL). For attenuation correction, the transmission scan was first reconstructed using a maximum-a-posteriori (MAP) scaled gradient ascent algorithm, as described [7]. The prior consists of a multimodel probability distribution (favoring the known attenuation coefficients of air, lung and tissue) and a Gibbs prior to encourage local smoothness (the Huber prior was used). Ordered subsets were used as an acceleration technique, iteration scheme: 2i/36s 1i/24s. The transmission images were then forward projected to produce the attenuation correction. The emission scan was reconstructed with an ordered subset expectation maximization (OSEM) algorithm, where attenuation and normalization were included in the system matrix. Iteration scheme: 1i/16s 1i/12s 1i/4s 4i/2s 1i/1s. Post-smooth: a Gaussian filter with 6 mm FWHM. The reconstructed image matrix was 128x128 with zoom 1.5 and pixel size 3.4 mm.

Processing: The body contour was derived from the transmission images. A 30 to 40% threshold level appeared appropriate to assure exclusion of the bed. Sometimes air pockets within the bowel would remain, which were filled (figure 1). All voxels within the body contour were included. After rebinning of the data into larger voxels (to speed up processing) the algorithm generated time-activity-curves (TACs) for each individual voxel. Such a TAC was formerly called a dixel (dynamic pixel) in 2D [1,2], and can be represented as a vector. For our system implementation, the zooming, rebinning and summation of planes produced voxels of 6.8 x 6.8 x 7.3 mm^3. TACs were generated for all

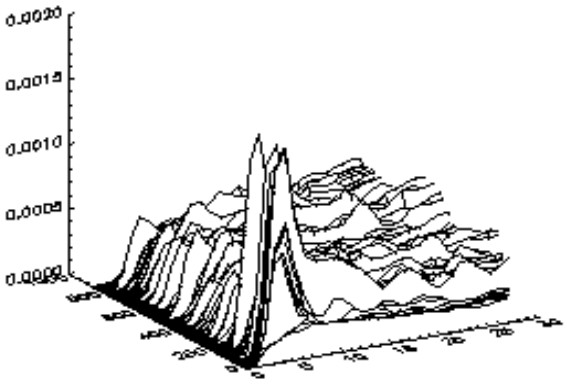

Figure 2. Set of TACs or vectors selected for processing. The x-axis indicates frame number, y-axis gives the 874 voxel TACs, and z-axis the magnitude in cnts/vox/sec. The peaks in the front correspond to the bolus passage through the arteries.

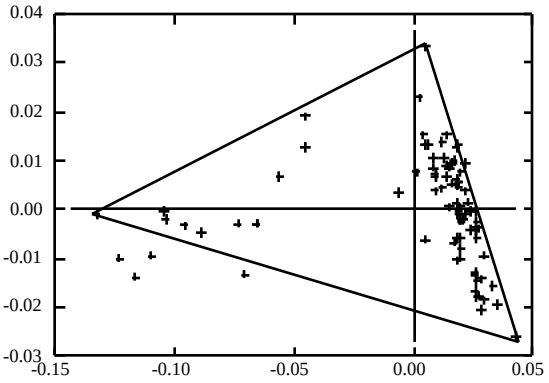

Figure 3. Hyperplane with the arrowheads (+) of the vectors in case of 2 principal components. The axes through the origin 0.00 are rotated obliquely. The three vertices of the triangle indicate the position of the 'pure' vectors or factors. The factors can be transformed back to the image space to create factor images.

voxels within the body contour, and comprised the complete vector set for the patient. Optionally, the magnitude of voxel TACs for further processing can be selected, e.g. between 50 and 100% of the maximum. Such 'histogram windowing' or 'thresholding' removes voxel TACs with a small magnitude (noise).

After smoothing with a temporal 1-2-1 kernel and normalization, principal component analysis (PCA) was performed, producing the principal axes in the hyperplane (figure 3). Using a non-orthogonal transformation, the principal components were rotated to obtain axes that have the maximum explained variance in the selected vector set. A SIMPLEX routine was used for fitting, and yielded vertices that constitute the factors of FA (see figure 3). Non-negativity of counts, i.e. factors are always positive, was used as constraint.

Thus, curves were produced that have the shape of the 'pure factor curves', but have incorrect magnitude due to the initial normalization step. Subsequently, the pure factors are transformed back to the image space, yielding factor images for each plane. The magnitude of the factor curves and factor images need adjustment to undo the initial normalization step. Scaling of the factors was done with two methods: 1) *reversed normalization*: multiplication by the initially used scalars that produced the normalized vectors (i.e. voxel TACs), 2) *image derived constants*: the pure factor images were used as masks for the delineation of an ROI with thresholding techniques. With this ROI and the original reconstructed PET images, an image based TAC was generated for the vessels and tumor. The image TAC was used to normalize the pure factor curve based on: 1) peak of the curve, 2) full area under the curve (AUC), 3) first half AUC, 4) second half AUC, 5) FWHM, or 6) FWTM of the initial peak.

In this way, 'pure' input and output curves are created which can be used for kinetic modeling. The standard UCLA three compartment model was utilized to calculate the micro parameters (k1-k4) and macro parameter (K) of the acetate uptake in the prostate cancer. The image interface, PCA, FA,

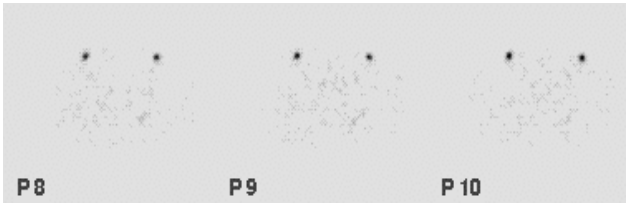

Figure 4. Transverse factor images representing the vascular phase of the acquisition. Note the high tracer uptake in both iliac arteries and the low background.

curve and image processing modules were written in IDL-5™. The kinetic modeling was done with non-linear regression routines and these were also written in IDL-5™. Processing of a typical study took 10-15 minutes on a SUN Ultra-5, and 5-8 min on an Ultra-60 workstation.

III. Results

By using 2 principal components three factors are generated with FA, i.e., a vascular factor (iliac vessels in the pelvis), a tumor factor (prostate cancer) and a residual. Figure 4 shows factor images of the iliac arteries in three adjacent planes. The vessels can be delineated with thresholding techniques, and the ROIs subsequently be used to generate an image based input function. The iliac vessels have a lumen of 3-6 mm and suffer from partial volume effects in the reconstructed images. The same procedure to derive a tumor ROI and generate an output function, was followed for the prostate tumor.

Figure 5 shows an example of an input curve of the blood vessels in the pelvis (left), and an output curve of the prostate tumor (right). The factor curves are generally smoother than the image based TACs. The 'pure' vascular factor curve or input function was normalized (scaled) using the FWHM of the peaks. The tumor TAC was generated with a mask obtained by thresholding the tumor factor image. The tumor ROI was comprised of those voxels within the tumor mask that contain 70% or more of the 'pure' tumor factor. The tumor factor curve was then scaled by using the integral (total area under the curve) of the image based tumor TAC. Figure 6 shows a summed image of the last 10 minutes of the dynamic acquisition (top) and the tumor factor image (bottom). Comparison shows the bilobular prostate gland in the summed images (e.g. plane P9, top row figure 6). The factor images reveal the cancer inside the right lobe of the prostate gland (see planes P10-11, bottom row of figure 6), because of the different behavior in time of normal and cancer tissue.

Reliable factor curves were obtained in 5/6 primary and 3/3 recurrent prostate cancer patients, yielding a success rate of 8/9 or 89% for automatic processing. The failure was related to bladder uptake, highly unusual for this tracer. For this latter patient, the contribution of bladder activity was removed by manual masking, which resulted in more realistic input and output functions.

In addition, semi-automatic regions were generated, using summation of the early images around the bolus peak, and late images of the last 10 minutes. Thresholding techniques within a manually drawn mask were utilized to create the ROIs and to generate the TACs. The image based input functions, generated either automatically by FA or semi-automatically by masking, were nearly identical. The tumor curves, however, were usually different, dependent upon number of principal components chosen and number of factors assigned to the prostate gland by FA, e.g. both tumor and normal tissue, or the contribution of the vascular factor in the prostate gland.

Table I shows the average number of vectors (i.e., voxel TACs) that were generated for the group of 9 patients. Plane averaging in the z-dimension and rebinning in the x and y-dimensions were used to arrive at the final voxel size of 6.8 x 6.8 x 7.3 mm^3. Low magnitude vectors were excluded, i.e., <50% of the maximum for the vascular subset and <30% or <40% of the maximum for the tumor subset. The bolus passage produced vectors of large magnitude and varying the lower window from 40 to 70% had no significant effect. The contrary was seen for windowing in the tumor subset. A decrease of 10% in the lower window, yielded an increase of 5-6% in vectors. A lower window >40% resulted in coarse sampling of the available tumor vectors. As a consequence of the increase in number of vectors, the explained variance decreased by a similar amount. Increasing the number of principal components by 1 yielded a 4-5% gain in explained variance.

In general, studies yielding >75% explained variance produced accurate results. As shown in Table I, only a small subset of all the vectors within the body contour was selected for further processing. In order words, most of the vectors

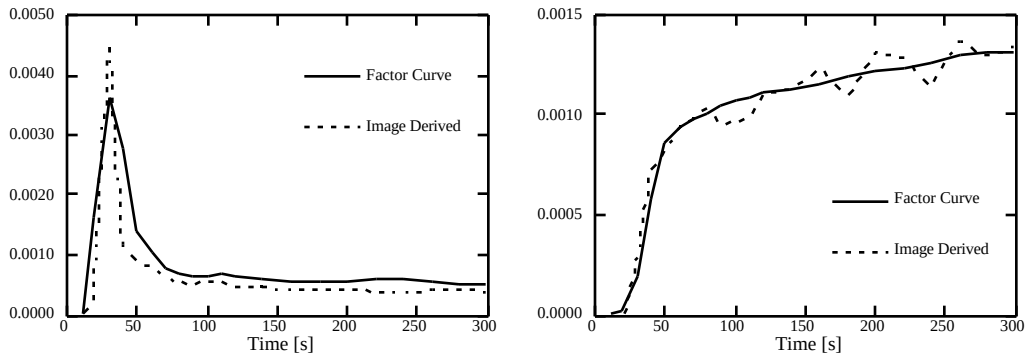

Figure 5. Input function or vascular curve (left panel) and output function or tumor curve (right panel). In general, the factor curves are smoother and 'less noisy' than the image derived curves.

TABLE I

Id	Tumor thr	Z rebin	Vectors N	Subset %	% Explained Variance 2-PCA	3-PCA	4-PCA
A	40%	*plane*	24856	4.1	80.5	84.7	87.9
	30%	*plane*	24856	10.8	74.3	79.3	83.3
B	40%	*iso*	10217	2.5	81.9	86.0	89.2
	30%	*iso*	10217	6.2	75.7	80.8	84.7

within the body contour are of low magnitude and apparently do not contribute in the FA.

In an attempt to study the effect of routine reconstructions, the standard processing and reconstruction algorithms of the manufacturer (CTI, Knoxville, TN) were used. This comprised filtered back projection (FBP) for the transmission scan followed by segmentation and forward projection. The emission scan was reconstructed using OSEM with 2 iterations and 8 subsets, and weighted attenuation compensation plus scatter correction. The final voxel size with a zoom of 1.0 was 5.0 x 5.0 x 2.4 mm^3. The rebinning module in our FA implementation, optimizes for isometric sampling in three dimensions (or 'cubic' voxel sampling) during processing, yielding 10.1 x 10.1 x 9.7 mm^3 (*iso*) as volume elements to derive the vectors (voxel TACs). Table I compares the two processing methods. The UCLA-KUL reconstruction followed by FA with plane summation (*plane*) is indicated as method A (Id-A) and the standard OSEM 2i/8s reconstruction followed by FA-*iso* as method B (Id-B) in Table I. The total number of vectors is higher for method A than B due to the voxel size. The size of the selected subset appeared smaller in method B, but there was no appreciable effect on the percentage of explained variance.

With the standard 3-compartment model, the micro and macro parameters, i.e., diffusion rates between compartments, were estimated. k1 reflects the flow to the prostate tumor and K the metabolic rate of acetate. Three combinations of input and output functions were used: 1) both generated with FA, 2) input with FA and output image based, and 3) both image derived. The results of these three conditions were compared to those obtained with semi-automatically drawn masking ROIs. Table II gives the average values of the kinetic modeling for the two groups, primary cancer (6 patients) and recurrent cancer (3 patients).

TABLE II

Input function	Output function	Method A k1	Method A K	Method B k1	Method B K
Primary Prostate Cancer					
FA	FA	0.54	0.092	0.67	0.120
FA	Image	0.57	0.073	0.69	0.098
Image	Image	0.71	0.125	0.72	0.078
Semi	*Semi*	*0.72*	*0.115*	*0.82*	*0.096*
Recurrent Prostate Cancer					
FA	FA	0.63	0.057	0.58	0.154
FA	Image	0.53	0.069	0.68	0.183
Image	Image	0.59	0.129	0.79	0.167
Semi	*Semi*	*0.58*	*0.136*	*0.68*	*0.181*

The values for k1 are similar and not significantly different given the small sample sizes. The values for macro-K, on the other hand, vary significantly. The UCLA-KUL reconstruction method reveals differences between FA and image based functions, whereas the standard method B does not. The vascular factor curves were nearly identical for the two methods A and B, whereas the tumor factor curves looked similar, but showed serious deviations in some patients.

The correlation between estimated parameters with FA-based and image-based input and output functions supplied r^2 = 0.61-0.84 for macro K in primary cancer. Linear regression analysis furnished slopes significantly different from unity. A five-parameter kinetic model was also attempted, i.e. a correction term for the blood volume inside the tumor was introduced. However, this model yielded less favorable curve fits and parameter estimates. Therefore, only results of the standard 3-compartment model with four parameters are shown.

IV. DISCUSSION

An automated procedure for the generation of a vascular

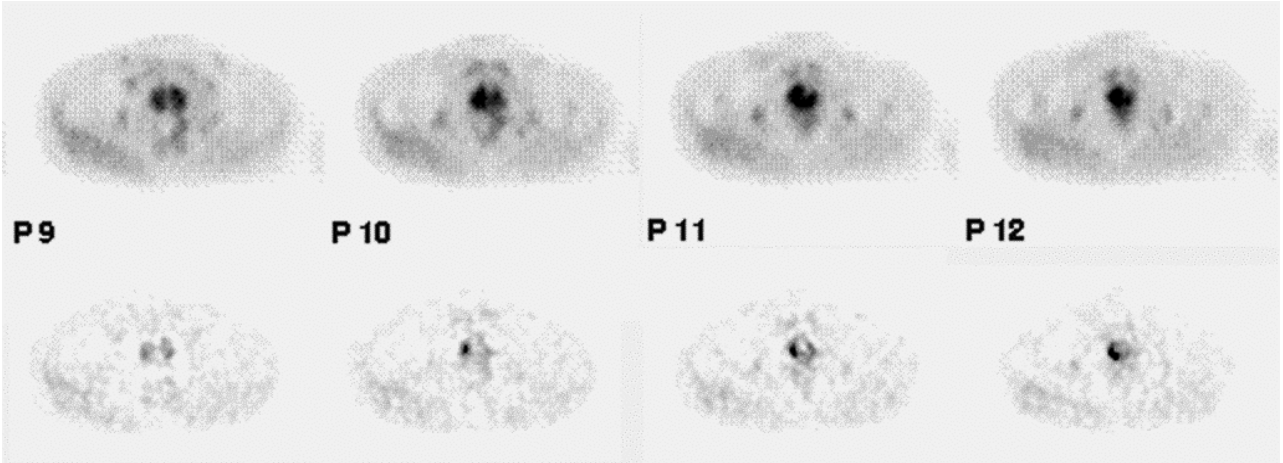

Figure 6. Top: summation of the last 10 min of the dynamic dataset. Note the bilobular prostate gland. Bottom: corresponding factor images. Note the tumor in the right lobe. The central photopenia on plane P11 bottom, is the urethra.

input function and a tumor output function, based on factor analysis of dynamic sets, was devised, written, coded and successfully implemented on a standard workstation. Reliable factor curves were obtained in 8/9 prostate cancer patients, a success rate of 89%. In one patient, there was uptake in the bladder, unexpected for ^{11}C-acetate, which could be related to an infection. Filling of the bladder is a major temporal change, readily picked up by FA. After masking the bladder by manual intervention, adequate input and output curves were obtained for this particular patient. This case example prompted the addition of modules to mask undesirable structures in the image set. Contrary to the common glucose analogue FDG, acetate is not excreted by the kidneys. Thus, there is no interfering activity in the bladder, located just above the prostate gland. This is the main reason for using acetate in prostate cancer.

Scaling of the factor curves was done here based on parameters of the reconstructed images. Earlier, we reported a method based on venous blood samples and obtained excellent correlations between the methods [5,6]. From a theoretical standpoint, 1 or 2 venous blood samples at the end of the study will suffice to 'calibrate' the tail of the input curve. This removes any partial volume and spillover effect. Such scaling of the input curve fails, however, if the measured activity within the vascular compartment contains so-called metabolites. When the administered freely diffusible tracer enters the cells, is metabolized and then released into the vascular compartment, a correction is necessary, i.e. measure the metabolites or correct with an average curve if similar across patients. The compartmental model for acetate in cancer, has not been studied in detail, but metabolism studies in the heart indicate a significant contribution of metabolites.

FA is extremely sensitive to noise artifacts, partially related to the normalization step. Therefore, a subset of vectors with sufficient magnitude is selected for further processing. The selection criteria are dependent of radiopharmaceutical, image reconstruction and sampling. The tracer uptake has to be different in time for the structures in the field of view, in order to be detected as different factors by FA. Noise can be reduced by iterative methods, which has a demonstrable beneficial effect on the created TACs as we reported earlier [8]. In a few patients, images reconstructed with FBP were used as input for the FA. Streak artifacts in the early low count images had a detrimental effect and generally produced inferior factor images. An effect of the reconstruction method is demonstrated in Table I. The UCLA-KUL method uses statistical methods, more iterations, and no segmentation when compared the manufacturer's method. This resulted in smoother looking images and a higher percentage of vectors selected.

Figure 6 reveals a potential application of clinical significance. FA could distinguish tumor from normal prostate tissue in this patient. The presence of tumor in the right lobe and absence in the left was confirmed by pathology in the surgical resection specimen. Analogously, FA may reveal tissue inhomogeneity and differentiation within the tumor. In other words, specific tumor components may be distinguished based on temporal patterns of tracer uptake.

The success rate of kinetic modeling was mixed in the current population. In 4/9 patients, the final fits showed deviations in the early phase. Therefore, a five-parameter model was attempted, which produced inferior results. These findings suggest that the standard 3-compartment model is not adequate for the acetate kinetics of prostate cancer. No validated model has been described for humans in the literature. More research into the acetate kinetics of cancer is necessary to elucidate the appropriate model.

The two processing methods A and B produced clear-cut differences in macro-K. Since the input functions of all the image based methods were nearly identical, the differences have to be attributed to the generated output functions. There is an obvious difference in re-sampling of data due to the voxel size. However, it is intriguing that the reconstruction methods produced different output functions and furnished higher values for K, especially in recurrent cancer. This deserves further research.

Table II also suggests a difference between FA and image derived curves for method A. This can be partially explained by the re-sampling of the original pixels. Re-sampling 4x4 instead 2x2 transverse pixels into 1 new one, i.e. rebinning factor 4 instead of 2, will significantly speed up processing. As a side effect, small structures like the iliac vessels, are reduced in intensity or might be smoothed out completely. This effect could be demonstrated easily with our FA package.

V. Conclusions

In dynamic PET studies, an accurate input and output function can be obtained with Factor Analysis. The input and output functions generated with FA appeared similar to those generated with ROIs on the images. Kinetic Modeling with input from Factor Analysis or TACs generated from functional ROIs supplied parameters that revealed high correlations in this limited population. FA input functions permit reliable parameter estimation, an important finding for the evaluation of sequential studies such as therapy monitoring in cancer. Our FA implementation provides a standardized method for evaluating quantitative PET images, applicable to studies across institutions and therapeutic regimens.

VI. References

[1] Barber DC. "The use of principal components in the quantitative analysis of gamma camera dynamic studies" *Phys Med Biol,* **25**: 283-292, 1980

[2] Di Paola, R, Bazin JP, Aubry F, Aurengo A, Cavailloles F, Herry JY, Kahn E. "Handling of dynamic sequences in nuclear medicine". *IEEE Trans Nucl Sci*, **4**: 1310-1321, 1982

[3] Barber D, Martel A. "Factor Analysis revisited". *Eur J Nucl Med*, **19**: 467-468, 1992

[4] Wu HM, Hoh CK, Choi Y, Schelbert HR, Hawkins RA, Phelps ME, Huang SC. "Factor Analysis for extraction of blood time activity curves in dynamic FDG-PET studies". *J Nucl Med,* **36**: 1714-1722, 1995

[5] Schiepers C, Wu HM, Nuyts J, Dahlbom M, Hoh CK, Huang SC, Phelps ME. "Fluoride PET: is non-invasive quantitation feasible with factor analysis ?" *J Nucl Med,* **38**: 93P, 1997

[6] Schiepers C, Hoh CK, Dahlbom M, Wu HM, Phelps ME. "Factor analysis for delineation of organ structures, creation of in- and output functions, and standardization of multicenter kinetic modeling" *Proceedings SPIE* **3661**: 1343-1350, 1999

[7] Nuyts J, Dupont P, Stroobants S, Maes A, Mortelmans L, Suetens P. "Evaluation of maximum-likelihood based attenuation correction in positron emission tomography" *IEEE Trans Nucl Sci*, **46**: 1136-11411999

[8] Schiepers C, Nuyts J, Wu HM, Verma RC. PET with $^{18}F^-$ - Fluoride: effects of iterative versus filtered backprojection reconstruction on kinetic modeling. *IEEE Trans Nucl Sci*, **44**: 1591-1593, 1997